

Central European Journal of Energetic Materials

ISSN 1733-7178; e-ISSN 2353-1843

Copyright © 2025 Łukasiewicz Research Network – Institute of Industrial Organic Chemistry, Poland

Cent. Eur. J. Energ. Mater. 2025, 22(3): 380-408; DOI 10.22211/cejem/211369

Supporting Information is available in PDF-format, in colour, at: https://ipo.lukasiewicz.gov.pl/wydawnictwa/cejem-woluminy/vol-22-nr-3/



Article is available under the Creative Commons Attribution-Noncommercial-NoDerivs BY NC ND 3.0 license CC BY-NC-ND 3.0.

Research paper

Low Signature Near-Infrared Illuminants Functionalized with Potassium, Rubidium, and Cesium Ion Salts

Yi Wang^{1,*)}, Xiaolan Song²⁾, Chongwei An²⁾, Fengsheng Li³⁾

- 1) School of Materials Science and Engineering, North University of China, Taiyuan 030051, China
- ²⁾ School of Environment and Safety Engineering, North University of China, Taiyuan 030051, China
- ³⁾ School of Chemistry and Chemical Engineering, Nanjing University of Science and Technology, Nanjing 210094, China
- * E-mail: wangyi528528@nuc.edu.cn

ORCID Information:

Xiaolan Song: https://orcid.org/0000-0001-7870-4874 Yi Wang: https://orcid.org/0000-0002-9823-6286

Abstract: Eight low signature near-infrared illuminants, with potassium nitrate, potassium perchlorate, rubidium nitrate, cesium nitrate, and/or cesium carbonate as the oxidizer(s) and infrared radiation source(s), were prepared via the mechanical mixing method. The micromorphology, thermal reactions, and safety of these materials were evaluated. In particular, as a focus of this work, their combustion performance was investigated via a combinatorial method using a visible and near-infrared light spectrometer (380-1050 nm), a thermal infrared camera, and a high-speed camera. The results indicated that, owing to the use of mechanical mixing, although the ingredients had different particle sizes, they were mixed very homogeneously, which was confirmed by their scanning electron microscopy (SEM) images. The safety of all the energetic composites was very high, as their impact and friction sensitivities were very low and their thermal sensitivity were also low. The differential scanning calorimetry (DSC) data revealed that all the composites had low reaction temperatures, high activation energies, and high thermal stability. Most importantly, regarding the combustion performance, the infrared radiations for all eight composites were very high, but their visible light emissions were very weak. These findings indicate that prepared infrared illuminants have good stealth effect. In the combustion flame of the composites, the gaseous potassium, rubidium and cesium atoms emitted strong near-infrared radiation, but these infrared lights had different wavelengths. In general, the simultaneous use of potassium nitrate, potassium perchlorate, rubidium nitrate, and cesium nitrate as composite oxidizers resulted in excellent infrared emission and poor visible light emission, as well as a moderate burning rate, which meets the requirements for invisible infrared illuminants. These data will be highly valuable for guiding the formula modification of composites in the future.

Keywords: near-infrared illuminant, low signature, potassium, cesium, rubidium

1 Introduction

Invisible infrared illuminants are pyrotechnic composites that burn and emit extremely high amounts of radiation in the near-infrared region (0.7-1.3 μ m) and very low luminescence in the visible light region [1-3]. They are used to manufacture various types of infrared lighting flares and infrared lighting equipment, enabling a substantial increase in the sight distances of active infrared night vision devices and low-light night vision devices. The invisible infrared illumination bomb is a new concept developed in the late 1980s. The structure and working principle are essentially the same as those of ordinary lighting flares, except that the illumination torch is equipped with an infrared illuminant [4-8]. However, the combustion of the infrared illuminant studied in [4-8] results in a large amount of near-infrared radiation. It is ineffective for traditional thermal imaging devices operating in the mid-infrared region.

In 1989, Thiokol Corporation in the United States developed the M-257 invisible infrared illumination bomb launched by a 70 mm aviation rocket. The spectrum of the light emitted by the flame was mainly concentrated within 0.5-1.1 μ m (especially within 0.7-0.8 μ m) [9, 10]. When the density of the infrared illuminant was controlled to 1.70-1.80 g/cm³, the infrared radiation intensity was approximately 1060 W/s, and the visible light emission intensity was approximately 3000 cd, which was equivalent to hanging a 100 W incandescent lamp at an altitude of 500 m.

The luminous intensity of ordinary visible light flares is approximately 1×10^6 cd. Therefore, on the battlefield, it is difficult for the enemy to detect where an infrared flare was fired. Usually, infrared flares with parachutes can burn in

the air for approximately 200 s. When a helicopter pilot carries the M912A night vision system, the infrared light emitted by the burning column illuminates the area 1000 m away [11, 12]. That is, the pilot's recognition distance is 15 times greater than that in the case without illumination. In addition, Thiokol Corporation also developed other types of infrared illumination flares, some of which are fired by mortars, some by howitzers, and some by airplanes. Overall, the use of invisible infrared flares has greatly enhanced the night combat capabilities of field troops.

Obviously, many of the specific formulas for these compositions have not been widely published by the U.S. military or other countries to prevent adversaries from defeating or exploiting any weaknesses in these systems. Currently, only a few studies have reported the specific formulas for invisible infrared illuminants [13-15]. The known principle is that gaseous potassium atoms emit strong radiation in the near-infrared region and less luminous visible light [16-18]. However, our experimental results revealed that, in flames, the infrared radiation of gaseous potassium atoms is mainly concentrated between 700-800 nm, whereas the radiation between 800-1050 nm is very small. In addition, gaseous potassium atoms and sylvite emit small amounts of visible light. Another issue is that, in the current formula, to minimize the generation of visible light as much as possible, most of the composites use potassium nitrate (KNO₃) as the oxidizer [19, 20]. The advantages of KNO₃ are that it is cheap, easy to purchase, and has a low combustion temperature, which is very helpful for stealth performance. However, our preliminary experiments revealed that even if the mass fraction of KNO₃ reaches 78 wt.%, the composite, after being compressed into a column, cannot be ignited and cannot burn in a sustained manner. Hence, the use of only KNO₃ as the oxidizer in invisible infrared illuminants clearly cannot meet the requirements. Thus, in this work, we focused on the other two elements, i.e. rubidium and cesium, which both belong, along with potassium, to the IA group of the periodic table, namely, the alkali metal elements. Owing to having the same outer electronic structure as potassium atoms, gaseous rubidium and cesium atoms should also have strong infrared radiation, similar to gaseous potassium atoms; in particular, there is hope to compensate for the infrared radiation between 800-1050 nm and reduce the amount of visible light that is emitted. The luminescence principle of rubidium and cesium elements during combustion is the same, that is, during combustion, they almost do not emit light in the visible light region, but have strong infrared radiation in the near-infrared region. Especially, for rubidium and cesium atoms, the wavelength of near-infrared radiation is higher than that of potassium atoms. These infrared radiations are the great supplement to that of potassium atoms. This is the basic principle of the combustion and luminescence of rubidium and cesium atoms. Moreover, adding suitable amounts of RbNO₃ and CsNO₃ to the formulation may improve the ignition and combustion performance of the compressed columns. Therefore, herein, revealing the effects of rubidium and cesium on the infrared radiation performance of illuminants is the focus.

2 Experimental

2.1 Materials

Benzoic acid ($C_7H_6O_2$), amorphous boron powder ($d_{50}\approx 1~\mu m$), cesium carbonate ($C_{52}CO_3$), ferric oxide ($F_{62}O_3$, $d_{50}\approx 1~\mu m$), and scaly graphite powder (200 mesh) were obtained from Sino Pharm of China. KNO₃, rubidium nitrate (RbNO₃), cesium nitrate ($C_{50}NO_3$), potassium perchlorate (KClO₄), and nitrocellulose (NC) with a nitrogen content of 12 wt.% were purchased from Gansu Yinguang Chemical Factory.

2.2 Preparation of the grains

The specific formulas for the six invisible infrared illuminants (III-1, III-2, III-3, III-4, III-5 and III-6) are shown in Table 1. There were also tested two other samples, *i.e.* III-7 and III-8, for which Cs₂CO₃ was used as the cesium source. In China, CsNO₃ is a special controlled chemical, whereas Cs₂CO₃ can be purchased at will. In particular, because it is unregulated by police, the price of Cs₂CO₃ is only one-fifth that of CsNO₃. Therefore, we also conducted detailed studies concerning the use of Cs₂CO₃ as a cesium source.

Table 1. Politicias for the infrared multimants									
Ingredient	Composition [wt.%]								
	III-1	III-2	III-3	III-4	III-5	III-6	III-7	III-8	
KNO ₃	78	_	30	_	_	10	_	10	
RbNO ₃		_		30	_	10	_	10	
CsNO ₃		- 30 10					_		
Cs ₂ CO ₃		_						10	
KClO ₄	_	- 78 48					68	48	
Benzoic acid		8							
Boron		3							
Fe ₂ O ₃		1							
Graphite		4							
NC		6							

Table 1. Formulas for the infrared illuminants

Grains of the six composites (III-1 to III-6) were prepared *via* the same method; thus, here, we mainly describe the method for the III-1 composition:

- 78 g of KNO₃, 8 g of benzoic acid, 3 g of amorphous boron powder, 1 g of Fe₂O₃, and 4 g of scaly graphite powder were added to a 500 mL small mechanical mixer. After preliminary mixing, the mixer was sealed. The material was mixed in the mechanical mixer for 45 min at a speed of 100 rpm, with forward and reverse rotations of 2 min each. The machine was stopped 45 min later, the material was extracted, and a mixed composite powder was obtained.
- 6 g of NC (as the binder for all the composites) was added to a 200 mL beaker containing 40 mL of acetone. After complete dissolution of the NC, 94 g of the mixed composite powder was added to the beaker and stirred thoroughly to form a uniform paste. Then, the paste was poured into a culture dish. The samples were freeze dried for 10 h to obtain a molding powder of the III-1 composite. The dried material was slightly hard and had to be carefully ground into a loose powder with a mortar.
- 20 g of the III-1 molding powder was added to a stainless steel mold ($\Phi = 18$ mm), pressed with a pressure of 10 MPa (or 4 tons) and held for 5 min. First, the mold was coated with vaseline as a release agent. After the mold was pressed, a 20 g III-1 column was obtained.

2.3 Calculations

The NASA-CEA2 code was used to predict the combustion performance of all the composites, and the results are listed in Table 2. Table 2 shows that the oxygen balance (OB_{CO2}) of all the composites approach zero oxygen equilibrium. According to the principles of traditional pyrotechnic chemistry, composites with a slightly negative oxygen balance exhibit excellent pyrotechnic effects. As shown in Table 2, for the adiabatic flame temperature (T_{ad}) , the evaluation results were basically ideal because, except that for III-1, all temperatures were approximately 2000 °C. It has been reported in the literature that a temperature of 2000 °C is sufficient for heating potassium, rubidium and cesium atoms, and their compounds into a gaseous state. These gaseous atoms and compounds are continually heated into their excited states and then fall back to their ground states, emitting large amounts of near-infrared light and some visible light [21]. Carbon monoxide, carbon dioxide, water vapor, and hydrogen chloride also emit infrared light, but the wavelengths of the infrared light are concentrated mainly in the mid-infrared and far-infrared regions, which is not suitable for active infrared night vision devices and low-light night vision devices, i.e. it benefits only traditional thermal imaging devices.

Danamatan	Sample									
Parameter	III-1	III-2	III-3	III-4	III-5	III-6	III-7	III-8		
Enthalpy [kJ/kg]	-4277	-2890	-3424	-2965	-2736	-3042	-2928	-3131		
OB _{CO2} [%]	-4.49	0.68	-1.31	-5.04	-7.02	-4.45	-3.94	-6.51		
T _{ad} [°C]	1534	2516	2388	2471	2495	2460	2514	2423		
M _c [g/mol]	44.508	45.250	45.810	48.928	50.694	48.439	47.804	49.166		
M	ass fract	ions of	gaseous	combus	tion pro	ducts [w	t.%]			
CO	5.0	9.3	7.4	11.4	13.6	10.7	11.8	12.3		
CO_2	33.0	26.3	29.2	22.9	19.5	24.0	23.7	22.9		
H_2O	2.2	2.8	4.0	3.6	3.2	3.7	3.0	3.7		
HC1	0	4.3	0.6	1.6	2.1	1.4	3.6	1.3		
N_2	11.5	0.6	4.7	3.5	2.8	3.7	0.7	3.0		
KBO ₂	22.7	16.9	21.6	12.1	13.2	16.0	15.8	15.9		
КОН	17.4	0.2	1.2	0.3	0.2	0.4	0.2	0.4		
Cl·	0	3.0	0.2	0.7	0.9	0.6	2.0	0.4		
FeCl ₂	0	0.7	0.1	0.2	0.3	0.2	0.5	0.2		
KC1	0	25.7	23.8	13.5	12.8	16.9	21.3	16.9		
O_2	0	4.8	3.0	1.5	0.9	1.7	2.2	0.9		
K·	6.9	0.2	1.3	0.5	0.4	0.6	0.4	0.7		
HBO ₂	0	0	0	1.1	1.8	1.0	2.1	1.0		
Rb∙	0	0	0	0.5	0	1.7	0	0.2		
RbBO ₂	0	0	0	12.5	0	4.3	0	4.2		
RbCl	0	0	0	11.7	0	3.8	0	3.8		
CsBO ₂	0	0	0	0	11.8	3.6	3.9	4.3		
Cs·	0	0	0	0	0.3	0.1	0.1	0.1		
CsCl	0	0	0	0	14.0	4.8	6.4	5.7		

Table 2. Combustion performance predictions via the NASA-CEA2 code

2.4 Test methods

Differential scanning calorimetry (DSC), apparatus DSC-100, with heating rates of 5, 7, 10, and 15 °C/min was used to study the thermal decomposition of all the composites and the sample mass was 5 mg.

The micromorphologies of the composites were analyzed *via* field emission scanning electron microscopy (SEM), apparatus TESCAN MIRA LMS. An OHSP-350IR spectrophotometer was used in the spectral photometry tests (Hangzhou HOPOO Light & Color Technology Co., Ltd.).

The fiber optic light harvesting head of the OHSP-350IR spectrophotometer was placed into the darkroom of the combustion tower, 0.3 m away from the

composite grain, facing the center of the flame. A thermal imager (HT30-300010001) was used to measure and record the combustion flame temperature. The working band of thermal imager is mainly concentrated in the mid wave infrared (MWIR, 3-5 μ m) and long wave infrared (LWIR, 8-14 μ m) bands.

Photos of the combustion flame were captured by a high-resolution color industrial camera. The frame rate of the industrial camera is 3000 frames and the exposure time is 5 ms. A diagram of the experimental setup is presented in Figure 1.

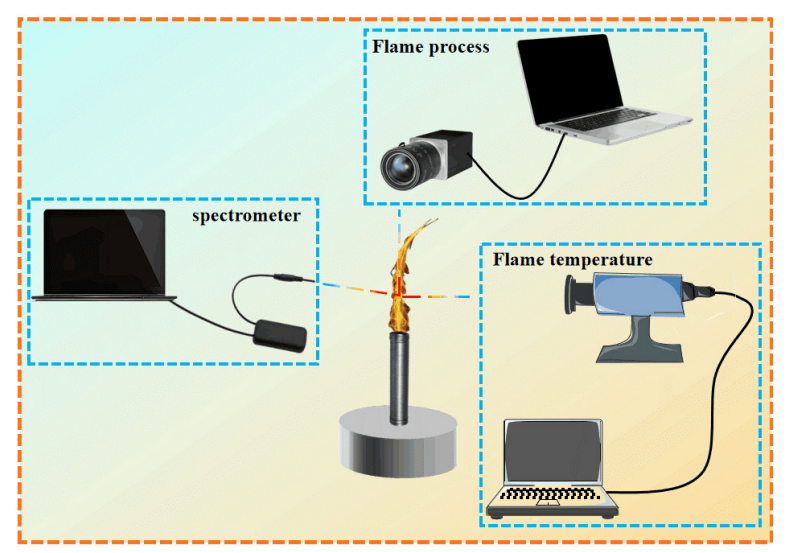


Figure 1. Experimental setup for testing combustion performance

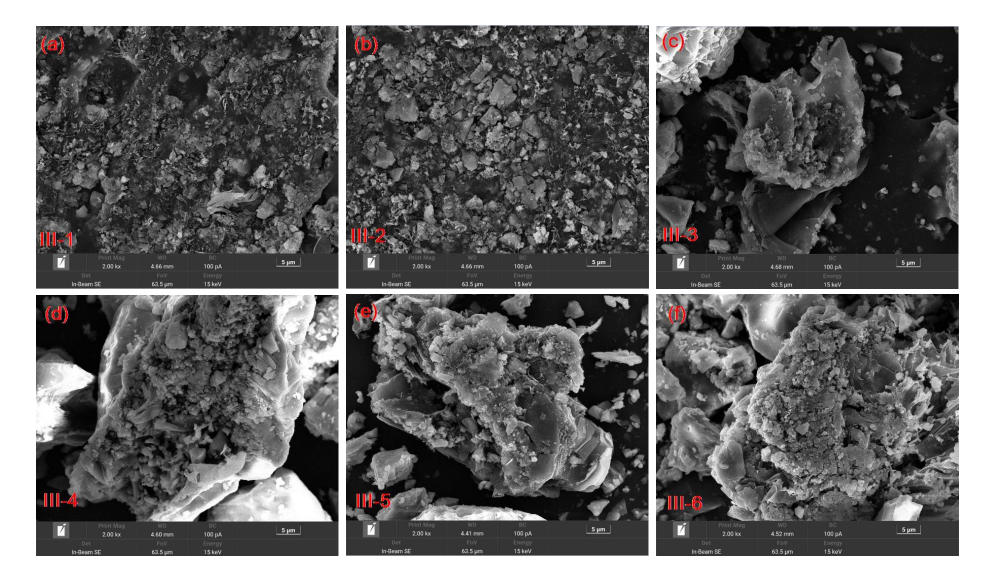
Impact sensitivity (H_{50}), in cm, of the composites was determined in compliance with GJB772A-97 method 601.2 (with a drop of 10 kg and a sample weight of 35 mg). The impact sensitivity instrument WL-1 was applied. The friction sensitivity (P), in %, of each composite was tested in compliance with GJB772A-97 method 602.1 (3.92 MPa, 90°, addition of 20 mg). The friction sensitivity instrument WM-1 was applied.

Thermal sensitivity tests, *i.e.* 5 s bursting point tests, were carried out in compliance with GJB772A-97 method 606.1.

3 Results and discussion

3.1 Characterization of samples

The microstructures of all the composites were tested via SEM, and the results are shown in Figure 2. Figures 2(a) to 2(h) indicate that, for the SEM images of III-1 to III-8, the microstructure of the pyrotechnics after mechanical mixing was different from that of the raw materials. However, from the SEM image in Figures 2(i) to 2(p), it can be seen that, for various raw materials, they had their own different microstructures rather than a mixture. The SEM image of the pyrotechnic charge was clearly a mixture, while the SEM image of the raw material was clearly a single substance. Due to the large number of substances involved in each formula, it was difficult to demonstrate that the pyrotechnic mixture was very uniform. However, it can be seen that all eight tested samples were relatively evenly mixed mixtures, which met the standards for further research. The XRD patterns of all raw materials and samples are shown in Figure 3. The eight graphs in Figure 3 indicate that, from III-1 to III-8, the XRD patterns of each mixture were consistent with those of its raw materials. Of course, due to the different amounts of each raw material added, the peak intensities exhibited in the XRD pattern of the mixture were not consistent, but the peak positions were the same. Therefore, Figure 3 illustrates that, through simple mechanical mixing in this work, the crystal phase of the raw material did not change.



Copyright © 2025 Łukasiewicz Research Network - Institute of Industrial Organic Chemistry, Poland

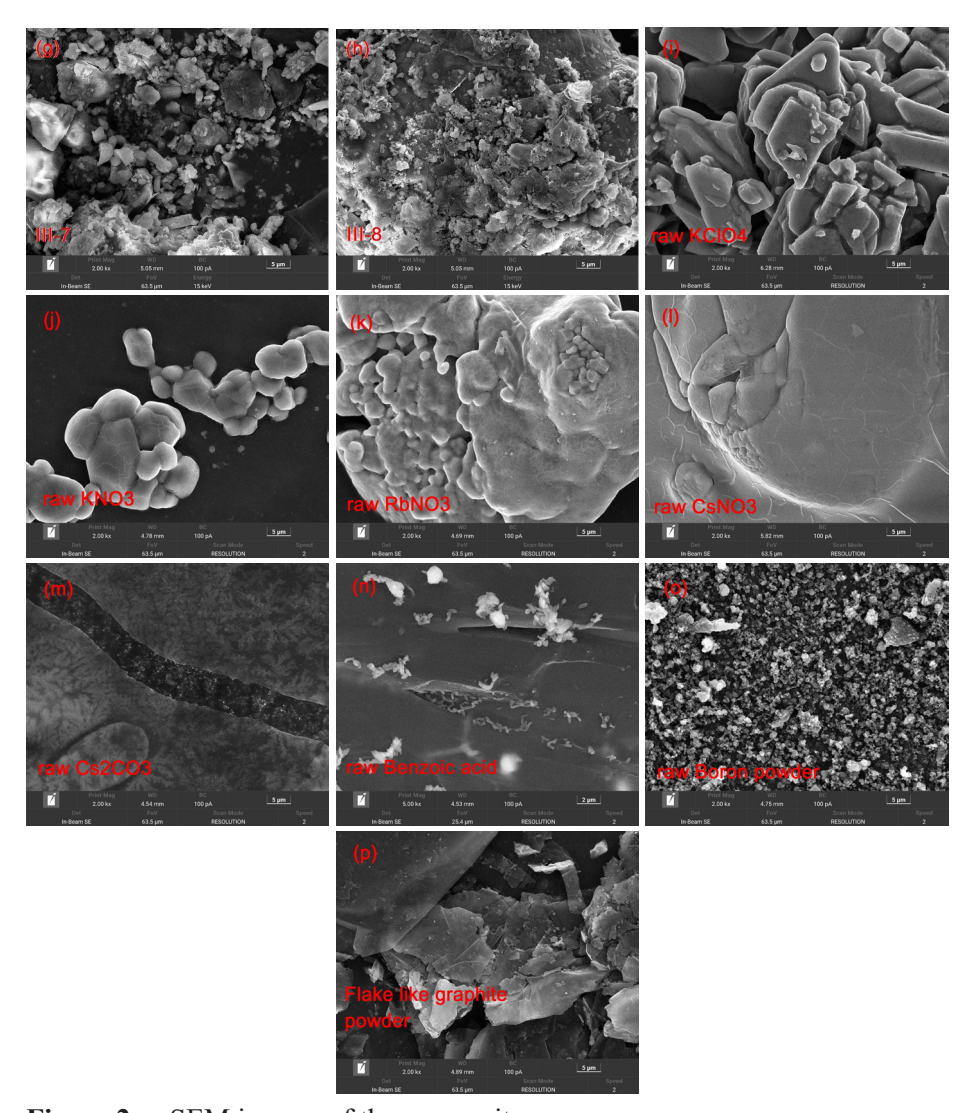


Figure 2. SEM images of the composites

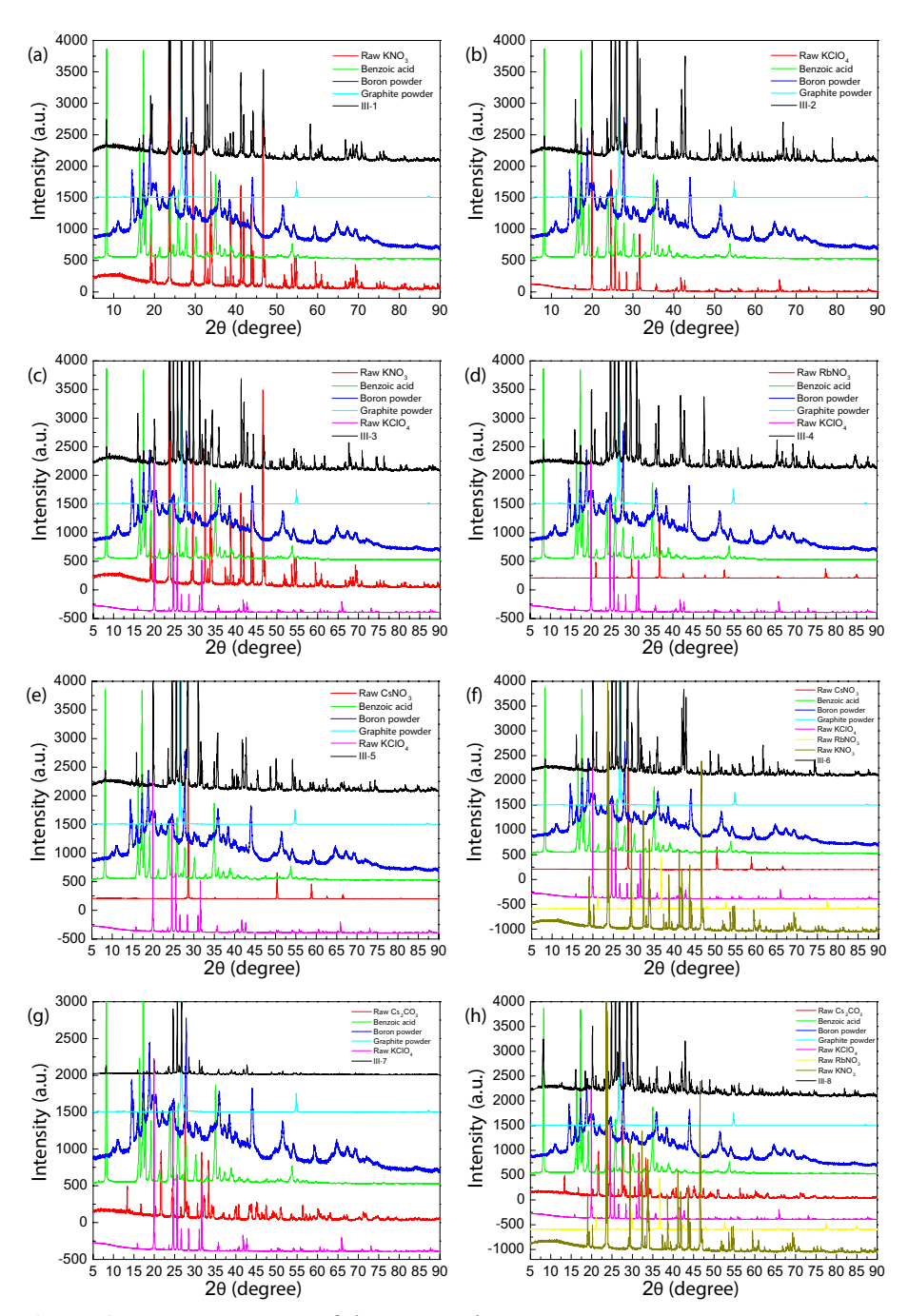
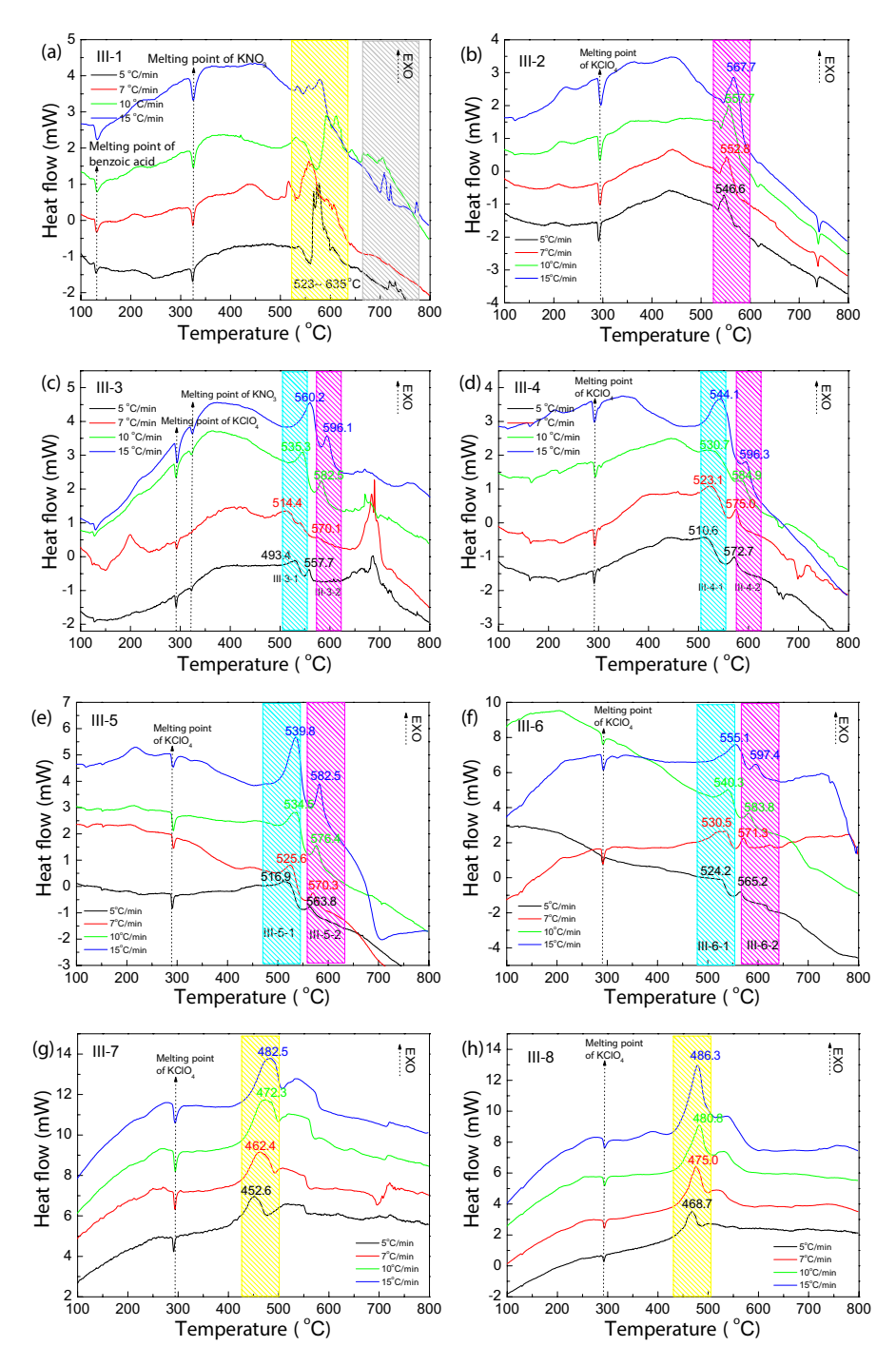


Figure 3. XRD patterns of the composites

3.2 Thermal reactions of the composites

The reactivities of all eight composites were investigated via DSC analysis, and the results are shown in Figure 4. The reason why we conducted DSC testing on eight samples is to investigate the thermal decomposition process of different oxidizers and their redox reaction processes. The objectives of the test was to predict and interpret the thermochemical properties of each pyrolant. Figure 4(a) shows the DSC curves of III-1 at different heating rates. The small endothermic peak that appeared at 326 °C corresponds to the melting process of KNO₃. There were several large exothermic peaks between 523 and 625 °C, corresponding to the redox reactions of the reagents of III-1. However, with increasing heating rate, the sizes and temperatures of these exothermic peaks did not change. The DSC results for III-2 are shown in Figure 4(b). In the DSC curve, the small endothermic peak at 293 °C corresponds to the melting process of KClO₄; compared with the endothermic peak of KNO₃ in Figure 4(a), the melting point of KClO₄ was slightly lower than that of KNO₃. The exothermic peak corresponds to the redox reactions between various substances in III-2. Figures 4(c-f) shows the DSC results for III-3 to III-6. The melting point of KClO₄ was still approximately 293 °C, but two exothermic peaks appeared on each DSC curve, corresponding to the oxidation-reduction reaction using nitrate and perchlorate as oxidizers. By comparing Figures 3(a) and 3(b), we can roughly conclude that the peak corresponding to III-3-1 is the exothermic process of decomposition of KClO₄, while the peak corresponding to III-3-2 is the exothermic process of decomposition of KNO₃. Although the nitrates include KNO₃, RbNO₃, and CsNO₃, the redox reactions using them as oxidizers only show one exothermic peak in each DSC curve.

III-7 and III-8 are composites that use Cs₂CO₃ as the cesium source, with only KClO₄ as the oxidizer. Therefore, in the DSC curves of III-7 and III-8, there is only one exothermic peak on each DSC curve, corresponding to the redox reaction between KClO₄ and other organic fuels. For each composite, the peak temperature of the exothermic peak in its DSC curve gradually increases with increasing heating rate, which is the basic law of DSC testing.



Copyright © 2025 Łukasiewicz Research Network - Institute of Industrial Organic Chemistry, Poland

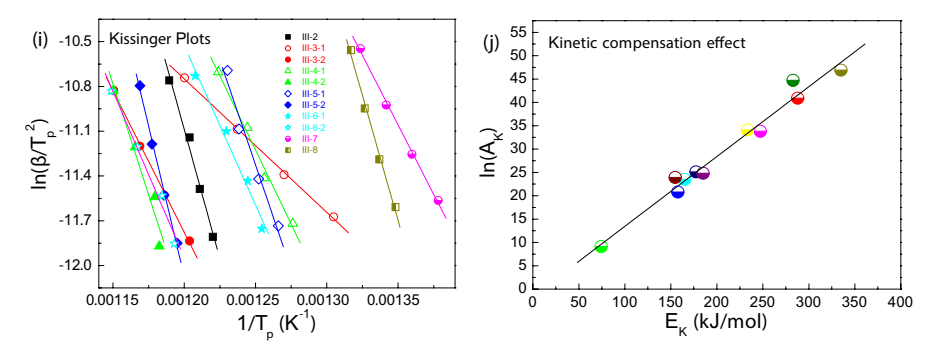


Figure 4. DSC curves of samples heated at different rates (a-h), the Kissinger plots (i) and the kinetic compensation effect (j)

The various thermochemical parameters for the thermal reactions of the six composites were calculated *via* Equations 1-7 [22], and the thermodynamic, kinetic, and thermal stability of their thermal decomposition were characterized.

$$\ln \frac{\beta}{T_p^2} = \ln \frac{R \cdot A_K}{E_K} - \frac{E_K}{R} \cdot \frac{1}{T_p} \tag{1}$$

$$k = A_K \cdot Exp\left(-\frac{E_K}{T_p \cdot R}\right) \tag{2}$$

$$A \exp\left(-\frac{E_K}{RT_P}\right) = \frac{K_B T_P}{h} \exp\left(-\frac{\Delta G^*}{RT_P}\right) \tag{3}$$

$$\Delta H^{\neq} = E_K - RT_P \tag{4}$$

$$\Delta G^{\neq} = \Delta H^{\neq} - T_P \Delta S^{\neq} \tag{5}$$

$$T_b = \frac{E_K - \sqrt{E_K^2 - 4E_K R T_{e0}}}{2R} \tag{6}$$

$$T_{e0} = T_{ei} - b\beta_i - c\beta_i^2 - d\beta_i^3 \tag{7}$$

where R is the gas constant (8.314 J·mol⁻¹·K⁻¹), T_p is the peak temperature in the DSC trace with a heating rate of 10 °C/min, K_B is the Boltzmann constant

 $(1.381\times10^{-23} \,\mathrm{J/K})$, h is the Planck constant $(6.626\times10^{-34} \,\mathrm{J/s})$, β is the heating rate (in °C/min); T_{ei} is the extrapolated onset temperature at a specific heating rate (in K); T_{eo} is the extrapolated onset temperature at the heating rate closest to zero (in K); ΔG^{\pm} is activation free energy (in kJ/mol); ΔH^{\pm} is activation enthalpy (in kJ/mol), ΔS^{\pm} is the activation entropy (in J/mol·K), Q is the theoretical decomposition heat per mole of explosive (kJ/mol), M is the theoretical mass per mole of explosive (in g/mol), $E_{\rm K}$ and $A_{\rm K}$ are the activation energy (in kJ/mol) and preexponential factor calculated via the Kissinger equation, respectively, and $T_{\rm b}$ is the critical temperature for thermal explosion (in K), which characterizes the thermal stability of the composites.

The results are shown in Figures 4(i), 4(j) and Table 3. Figure 4(i) shows that the $[1/T_p]$ - $[\ln(\beta/(T_p)^2)]$ values for samples III-1 to III-8 exhibit a good linear relationship with a linear correlation coefficient R² > 0.99, indicating that the activation energy and preexponential factor calculated from the DSC curve data are very accurate. The kinetic compensation effect in Figure 4(j) shows that the $[E_K-\ln(A_K)]$ points of the eight exo-reactions are on a straight line, indicating that their kinetic mechanisms of thermal reactions are consistent. This is understandable since all the exo peaks correspond to redox reactions between similar oxidizers and fuels. The kinetic data in Table 3 indicate that E_K of all the reactions is 69-283 kJ/mol, which is similar to the activation energy of ordinary pyrotechnic composites. Each composite has a moderate k value, indicating that its thermal reaction rate is low. The thermodynamic data indicate that the activation enthalpy (ΔH^{\neq}) of III-3-1 is almost the minimum value, indicating that the activation process requires the absorption of less heat. The activation enthalpy of III-5-2 is obviously higher than those of the other materials. The differences in the ΔG^{\neq} values of the eight samples are very small, and all the values are positive, revealing that the activation processes of the composites are nonspontaneous and require the absorption of heat to reach the activation state. All the ΔS^{\neq} values are positive, indicating that the number of degrees of freedom of the composites increases after activation and that gas generation should occur during the activation process. The T_b values for the six composites reached 454-618 K, which is close to those of pyrotechnic compositions in which nitrates and/or perchlorates are used as oxidizers. This means that the thermal stabilities of the eight composites are relatively high.

	$T_{\rm p}$ for	Th	ermodynai	Kir	Stability			
Code	10 °C/min	ΔH^{\neq}	$\Delta G^{\scriptscriptstyle emp}$	ΔS^{\neq}	$E_{\rm K}$	1m 1	k	T_b
	[°C]	[kJ/mol]	[kJ/mol]	[J/mol·K]	[kJ/mol]	$\ln A_K$	[s ⁻¹]	[K]
III-2	557.8	283.3	237.7	81.8	287.9	40.9	6.28	527.3
III-3-1	545.5	69.8	169.4	182.8	74.3	9.1	5.45	460.1
III-3-2	582.7	152.9	202.7	85.6	157.7	20.8	8.05	538.5
III-4-1	530.8	160.6	193.9	62.9	165.0	23.5	8.90	453.1
III-4-2	585	242.9	229.9	22.1	247.3	33.8	3.52	618.6
III-5-1	534.6	229.1	215.8	24.8	233.5	34.1	8.95	505.5
III-5-2	576.5	330.2	254.7	131.1	335.0	46.9	9.90	550.7
III-6-1	540.4	173.0	199.9	49.8	177.5	25.1	5.25	542.4
III-6-2	583.9	180.3	211.1	52.7	185.2	24.8	1.57	606.5
III-7	472.4	150.9	178.4	58.3	154.8	23.9	1.81	438.2
III-8	480.9	278.8	223.9	114.1	282.8	44.7	4.62	454.9

Table 3. Thermodynamics, kinetics, and thermal stabilities derived from DSC traces

3.3 Mechanical and thermal sensitivities of the composites

The impact, friction and thermal sensitivities of each of the eight composites were tested according to the national military standard, and the results are shown in Figure 4 and Table 4. Table 4 shows that, for all the tested samples, the impact sensitivity is very low. After a 10 kg drop hammer hit a 35 mg sample at a height of 150 cm, the results revealed that none of the samples had reacted, exploded, or burned. The colors and smells of all the measured samples did not change before versus after testing. Thus, none of the color composites are sensitive to external impact action. The results of the friction sensitivity tests are different from those of the impact sensitivity tests. Under a 90° swing angle and pressure of 3.92 MPa, almost all the samples reacted. Since composite III-1 contains only KNO₃ as the oxidizer, its friction sensitivity is very low. We know that KNO₃ is the mildest oxidizer in fireworks because of its high melting point and substantially endothermic heats during its thermal decomposition. During the testing processes of III-2 to III-8, these seven samples had a slight odor release after testing, but there was no explosion or combustion, and only a slight reaction occurred. For III-2, when KNO₃ was replaced with KClO₄, the explosion probability of the friction sensitivity suddenly increased to 20%. This occurred because KClO₄ is a "hotter" oxidizer than KNO3 is. Although its thermal decomposition is also a weakly endothermic process, the amount of heat absorbed is much less than that of KNO₃; moreover, the amount of heat released by the reaction between KClO₄ and fuel is much greater than that released by the reaction between KNO₃ and the same fuel. Therefore, the friction sensitivity of the composite with KClO₄ as the oxidizer is obviously greater than that of the composite with KNO₃ as the oxidizer. The explosion probabilities of the friction sensitivities of III-3, III-4, III-5, and III-6 were similar. These findings indicate that the friction sensitivities of RbNO₃ and CsNO₃ are similar to that of KNO₃ and that there is no remarkable discrepancy among them. For III-7 and III-8, the situation changed since their explosion probability decreased from approximately 20% to 8% (or 4%). This occurred because, for III-7 and III-8, we replaced CsNO₃ with an inert material, *i.e.* Cs₂CO₃. Cs₂CO₃ is a nonenergetic material, so its introduction obviously reduced the friction sensitivity of the composites. In general, in terms of intentional or unintentional stimulation by friction or impact, the sensitivities of all the composites were low, which is related to the fact that we did not use metallic powders (such as magnesium and aluminum) as the fuel.

Table 4.	Mechanical	and thermal	sensitivities	of the com	posites
----------	------------	-------------	---------------	------------	---------

Comple	II [am]	D [0/]	Thermal sensitivity		
Sample	H_{50} [cm]	P [%]	T_{5s} [°C]	E [kJ/mol]	
III-1	>150 (NE ¹⁾)	0, no reaction	287.5	28.4	
III-2		20 (S ²⁾)	284.2	44.2	
III-3		16 (S)	301.8	35.4	
III-4		20 (S)	292.0	27.1	
III-5		24 (S)	317.2	38.1	
III-6		20 (S)	302.8	32.3	
III-7		8 (S)	335.8	45.4	
III-8		4 (S)	292.9	42.3	

¹⁾ NE – not exploding, ²⁾ S – smell something

The thermal sensitivity of all eight composites was tested via burst point experiments, and the results are shown in Table 4 and Figure 5. The calculation methods for the 5-s burst point, T_{5s} , and activation energy, E, can be found in reference [22]. T_{5s} clearly lies within 284-335 °C, and there is no marked difference in the T_{5s} among the samples. This reveals that the thermal sensitivity of the composites does not vary remarkably after the replacement of KNO₃ with KClO₄. The T_{5s} values of III-3~III-6 indicate that the addition of RbNO₃ and CsNO₃ did not cause significant changes in T_{5s} . For III-7 and III-8, although inert Cs₂CO₃ was used instead of energetic CsNO₃, there was still no considerable change in T_{5s} . The change in E followed the same pattern as the chang

the eight samples do not possess similar kinetic mechanisms. Overall, the thermal sensitivity of these samples is low and is similar to that of traditional color composites.

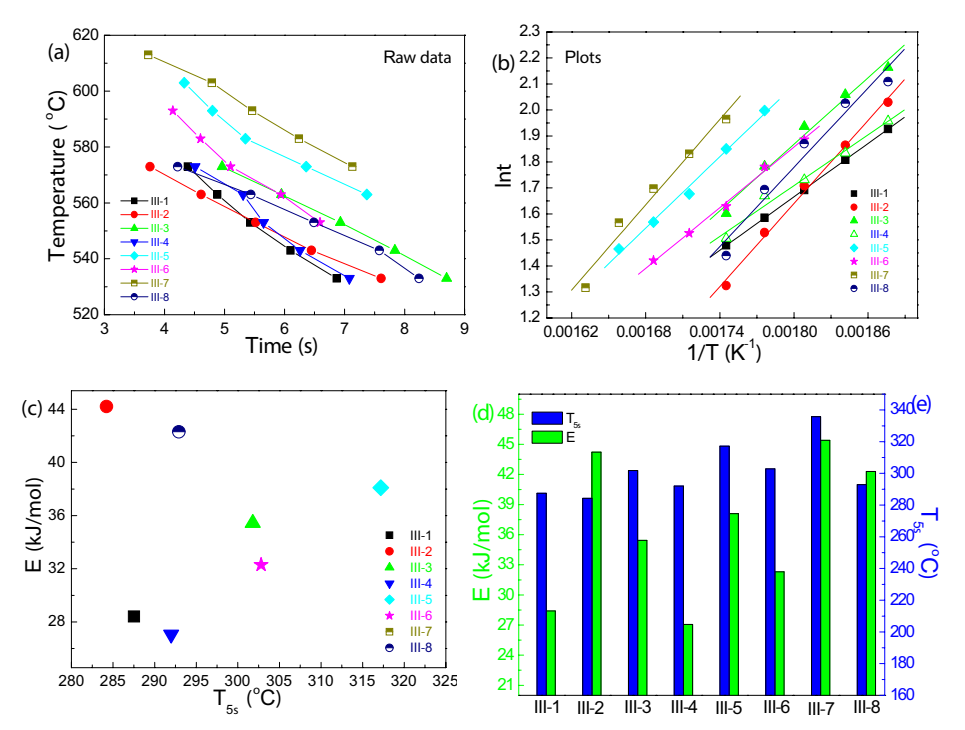


Figure 5. Thermal sensitivity of the colored composites: the raw data (a), the plots (b), relationship of T_{5s} to E (c) and the comparison of E and T_{5s} (d)

3.4 Combustion performance

3.4.1 Spectrogram analysis

The spectrograms are the most important data in this study and display the visible and near-infrared light (380-720 nm) emitted by the combustion flames of the composites. The results are shown in Figure 6 and Table 5. Figure 6(a) reveals that, for III-1, a strong emission peak appears at 724-821 nm. Obviously, this peak is located in the near-infrared region and does not correspond to visible light. In the visible light region, there is only a weak Na⁰-D peak, which is caused by impurities in the KNO₃ reagent. In the periodic table, sodium, K, Rb, and Cs are elements in the IA group, making it difficult to completely remove them

entirely. Thus, in all the spectra in Figure 6, a very weak Na⁰-D peak exists at approximately 589 nm. However, this peak is extremely small, and the yellow light emitted by Na⁰-D is extremely weak and can be ignored. The situation in Figure 6(b) is basically consistent with that in Figure 6(a). For III-2, there is also no emission peak in the visible light region and a very large radiation peak in the near-infrared region. Moreover, the locations of the infrared peaks of III-1 and III-2 are the same, namely, 786.3 nm. This finding indicates that the position of the infrared peak is the same for both KNO₃ and KClO₄. However, the irradiance of III-2 at 786.3 nm is 2478 (mW)/m²·nm, whereas the irradiance of III-1 at 786.3 nm is only 534 (mW)/m²·nm. The main reason for this substantial discrepancy is that the flame temperatures of the two compositions are different, which is discussed in the next section of this paper. The emission spectrum of III-3 is similar to those of III-1 and III-2, and owing to their similar formulations, it will not be discussed here.

In Figure 6(d), for III-4, the situation has changed. At 781.2 and 795.6 nm, two sharp infrared radiation peaks appeared, corresponding to the excitation and decay, respectively, of the outer electrons in the gaseous rubidium atoms in the flame. The data in Table 5 indicate that, for III-4, the intensity of the K⁰ peak reached 4001 (mW)/m²·nm, and the intensity of the Rb⁰ peak also reached 3179 and 2228 (mW)/m²·nm. This finding revealed that the introduction of RbNO₃ not only increased the infrared radiation range of the composite but also increased the infrared radiation intensity. In Figure 6(e), for III-5, after the replacement of RbNO₃ with CsNO₃, two new sharp peaks appeared at 852.4 and 895.1 nm, which correspond to the infrared radiation of gaseous Cs⁰ atoms in the flame. This implies that the introduction of CsNO₃ further expanded the infrared radiation range of the composite. Moreover, the introduction of CsNO₃ did not reduce the intensity of the infrared radiation peak, which is a very positive signal. As shown in Figures 6(g) and 5(h), in the formulas for these two composites, Cs₂CO₃ was used instead of CsNO₃ to reduce costs. Cs₂CO₃ is an unregulated chemical that is easy to purchase and much cheaper than CsNO₃. The data in Table 5 indicate that the position of the infrared spectrum did not change after the replacement of CsNO₃ with Cs₂CO₃, but the intensity of the infrared radiation peak decreased significantly, which is not beneficial for the practical use of the composite. The reason for this phenomenon is undoubtedly related to the decrease in the flame temperature.

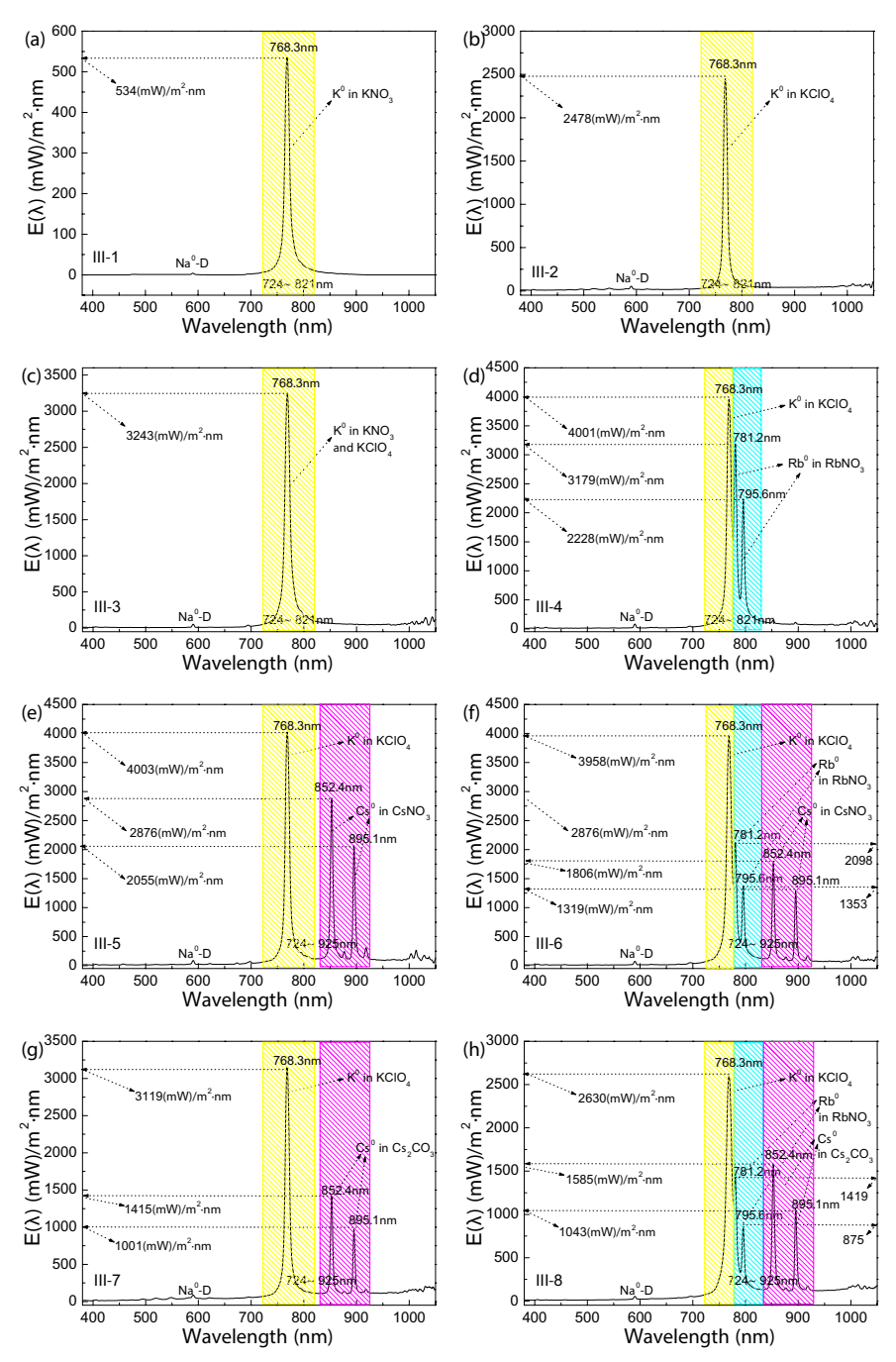


Figure 6. Infrared spectra of flames for different composites

Copyright © 2025 Łukasiewicz Research Network - Institute of Industrial Organic Chemistry, Poland

	Zummere em properties er umrerem vempesione							
C 1 -		irradia rared wa			Visible light	Infrared		
Sample	K^0	R	b^0	Cs^0		illuminance intensity [cd]	luminescence intensity [cd]	
	768.3	781.2	795.6	852.4	895.1	intensity [cu]	intensity [cu]	
III-1	534	0	0	0	0	1.2	11	
III-2	2478	0	0	0	0	26.3	276	
III-3	3243	0	0	0	0	14.5	124	
III-4	4001	3179	2228	0	0	23.0	211	
III-5	4003	0	0	2876	2055	29.5	271	
III-6	3958	2098	1353	1806	1043	20.7	190	
III-7	3119	0	0	1415	1001	52.8	484	
III-8	2630	1419	875	1585	1043	23.5	216	

 Table 5.
 Luminescent properties of different composites

Although Figure 6 does not show significant visible light emission (380-720 nm), it does not prove that their combustion does not produce bright and visible flames. During the tests, the visible light emission was very weak. Hence, we enlarged the spectra in Figure 6 and focused on wavelengths between 380 and 720 nm, from which we can clearly see visible light peaks. Figure 7(a) shows that there are distinct peaks in the blue light range (435-480 nm), green light range (500-560 nm), yellow light range (Na⁰-D), and red light range (620-720 nm). These emission peaks are intricate and span the entire visible light range. Thus, at the experimental site, the flames we observed were almost white in color. The chromatographic data were calculated via professional software, and the results are shown in Figure 7(b). Figure 7(b) shows that, except for the slightly green color of III-1, the flame colors of the other seven composites are basically white, which is consistent with the results we observed on site. In this study, we also captured color photographs of all the flames. However, overall, the visible light outputs of these eight infrared illuminants were extremely weak.

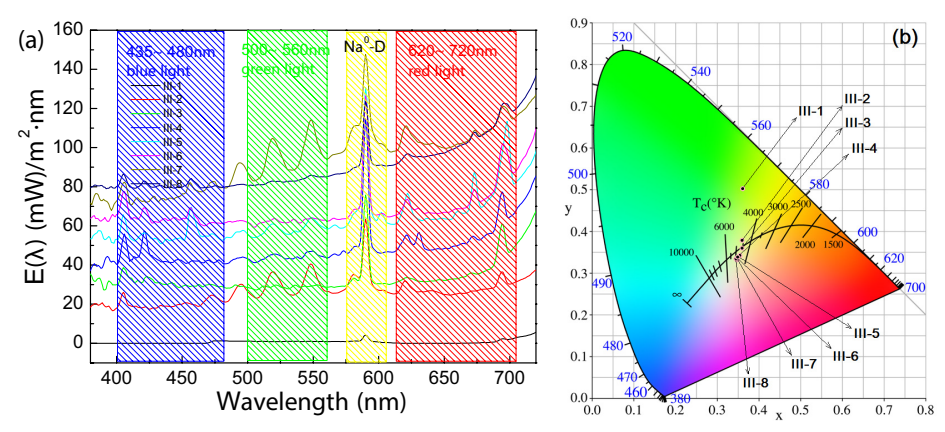


Figure 7. Visible light spectra (a) and chromatogram (b) of flames for different composites

3.4.2 Thermal infrared analysis

Using a high-resolution thermal infrared camera, we recorded the combustion process of each composite. The infrared photos of the combustion flames are presented in Figure 8, and the curves of the flame temperature with respect to time (*T-t* curves) are shown in Figure 9. In fact, Figure 9 not only presents these data but also provides accurate combustion durations of each composite. In the photos in Figure 8, the infrared radiation generated by the burning flames is very obvious. Moreover, the flame temperature gradually decreases from the inside out. Figure 8(a) shows that for III-1, the flames are roughly divided into three layers. The innermost layer has the darkest color, and the flame becomes lighter moving outward. If the darker the color is, the higher the temperature, then the outer edge of the flame should have a lower temperature, which reflects a deeper infrared radiation for the internal flame than for the outer flame. In fact, this result has been captured and confirmed by the high-speed photography in Figure 10, and this phenomenon is analyzed in that section.

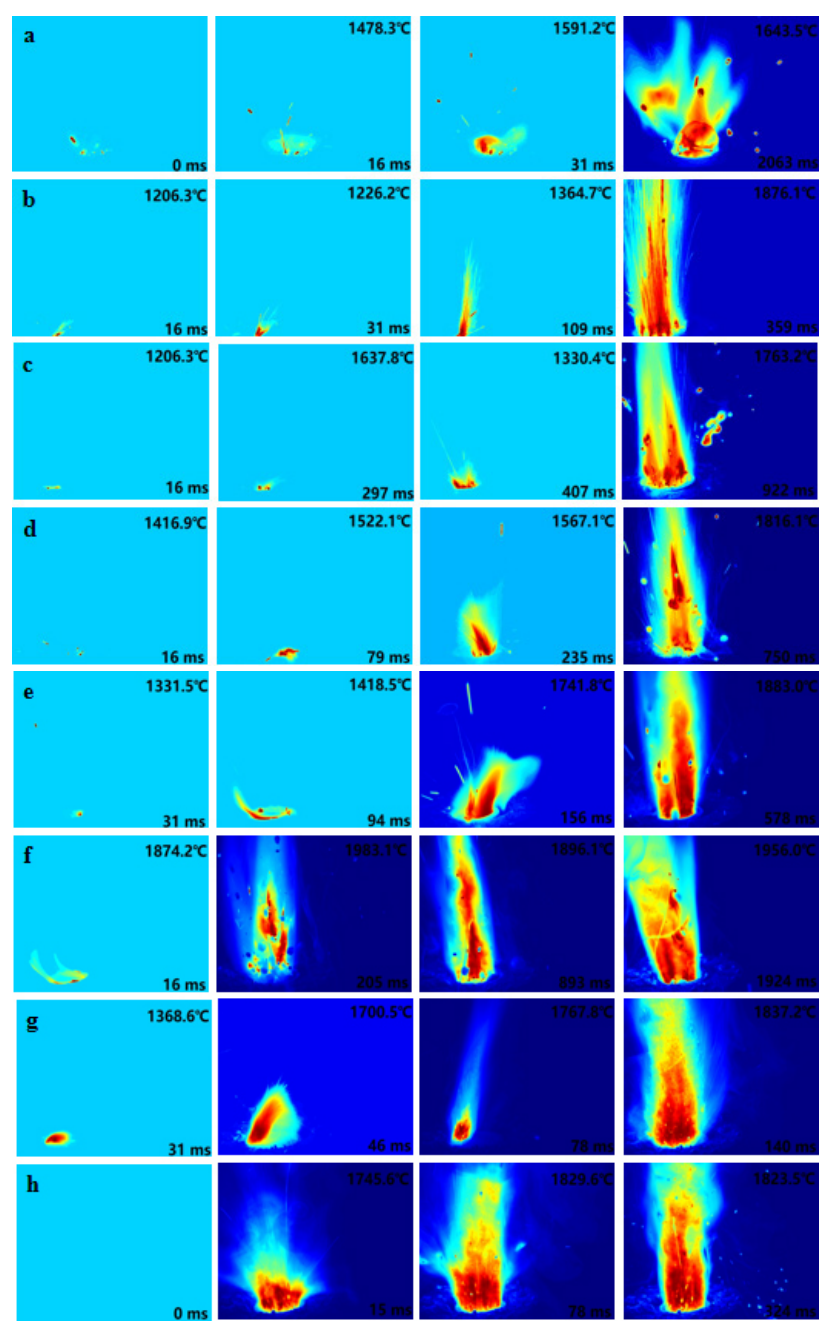


Figure 8. Thermal infrared images of the composites: III-1 (a), III-2 (b), III-3 (c), III-4 (d), III-5 (e), III-6 (f), III-7 (g) and III-8 (h)

Figure 9(a) clearly shows that the combustion of III-1 lasted for 50 s, and the average temperature of its flame was 1319 °C. For III-2, the burning time decreased to 22 s, and the average temperature of its flame increased to 1701 °C. The formula for III-1 uses KNO₃ as the oxidizer, whereas the formula for III-2 uses KClO₄ as the oxidizer. In fireworks, KClO₄ is a "hotter" oxidizer than KNO₃ is, so the composite using KClO₄ as the oxidizer should indeed have a higher flame temperature than that of the composite using KNO₃ as the oxidizer. Because III-3 is composed of both KNO₃ and KClO₄, its burning time and flame temperature were between those of III-1 and III-2. The combustion duration and flame temperature of III-4 were essentially consistent with those of III-3, which indicates that there was no significant change in the combustion performance of the composites when KNO₃ or RbNO₃ was used as the oxidizer. For III-5 and III-6, when CsNO₃ was introduced into the composites, their combustion durations became shorter, and the flame temperature increased. This implies that the oxidation ability of CsNO₃ is greater than that of KNO₃ and RbNO₃. Figure 6 also indicates that the composites with both KClO₄ and CsNO₃ as oxidizers emitted the strongest infrared radiation, which resulted from their highest flame temperature. However, even at the highest flame temperature, III-4 and III-5 did not have stronger visible light emission. That is, if the combustion duration is not considered, infrared illuminants containing CsNO₃ as the oxidizer will produce stronger infrared radiation during their combustion. In Figures 9(g) and 9(h), for III-7 and III-8, when Cs₂CO₃ was used instead of CsNO₃, the combustion durations of the composites decreased sharply, which means that the burning rate increased significantly. However, because of the lack of energy in Cs₂CO₃, the flame temperatures of III-7 and III-8 were slightly lower than those of III-6 and III-7.

In summary, our experimental results indicate that:

- to significantly extend the combustion time of the composite, KNO₃ should be used as the oxidizer separately,
- to increase the combustion temperature, KClO₄ should be used as the oxidizer,
- to expand the wavelength range of the infrared radiation, RbNO₃ and CsNO₃ should be used as the oxidizers, and
- to significantly increase the burning rate of the composite, Cs₂CO₃ should be used as the cesium source.

3.4.3 Flame color and structure analysis

We used a color high-speed camera to investigate the shapes and colors of the flames for all eight composites, and the results are shown in Figure 10, which presents representative flame photos at different burning times. Figure 10 shows

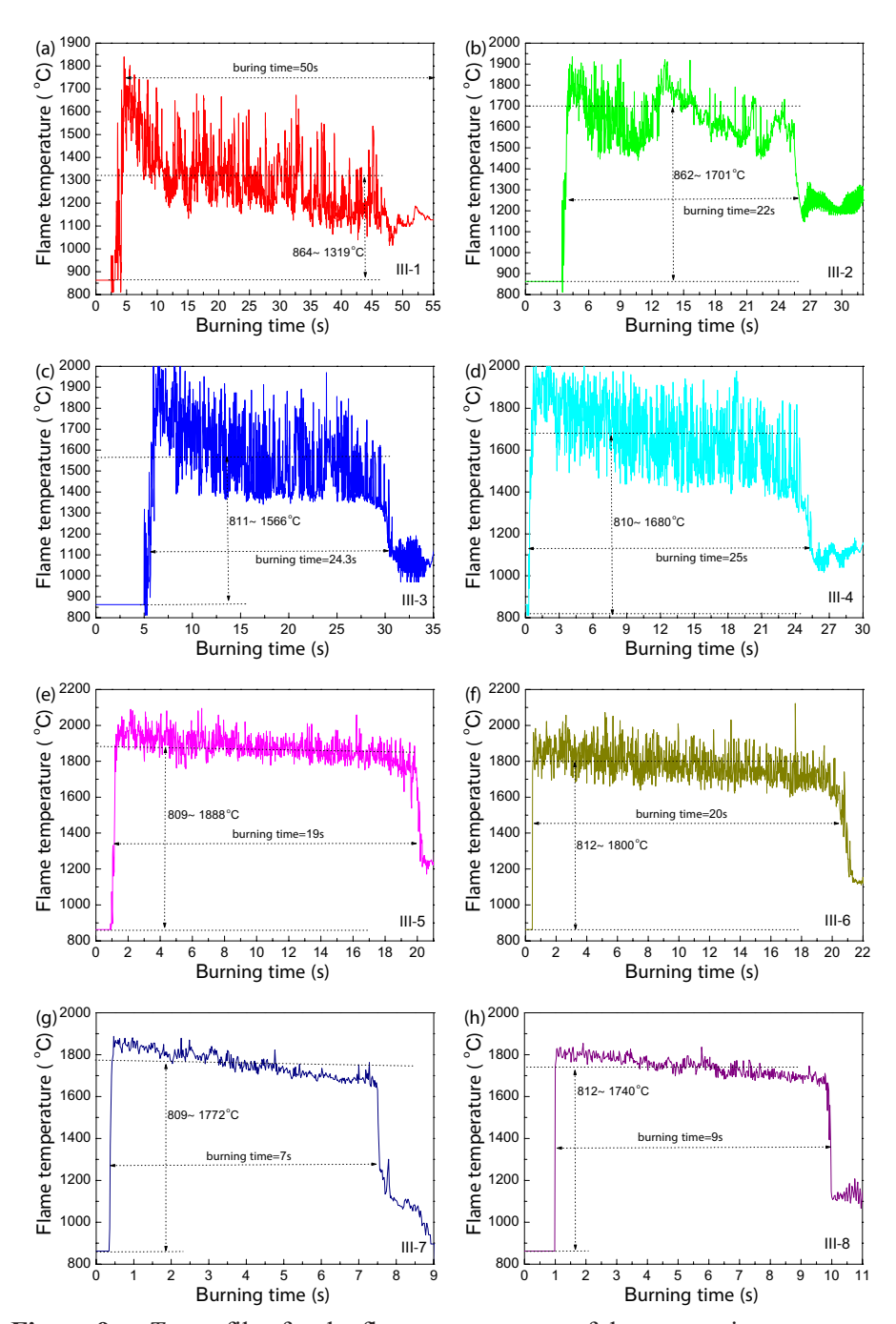
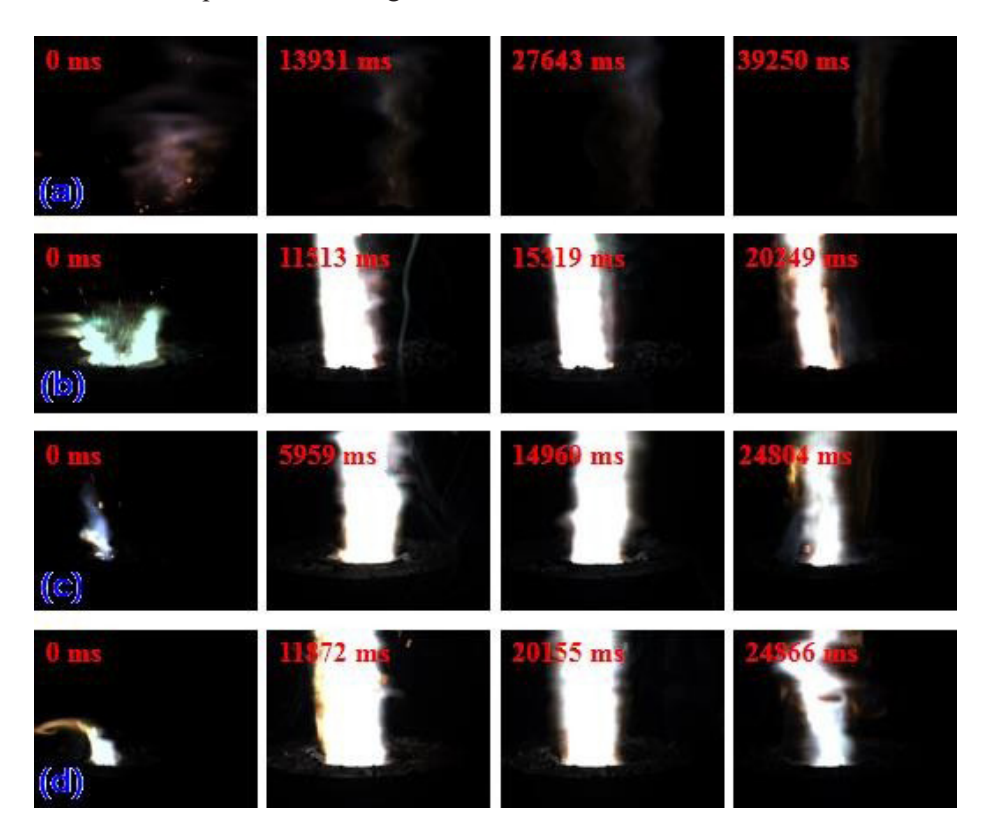


Figure 9. *T-t* profiles for the flame temperature of the composites

Copyright © 2025 Łukasiewicz Research Network - Institute of Industrial Organic Chemistry, Poland

that all the columns except that of III-1 had white flames, which is consistent with the data in Figure 7. For III-1, the color camera hardly captured its visible flames. However, in Figure 8(a), the infrared flames of III-1 are clearly present in the photos captured by the thermal infrared camera. This means that combustion of III-1 almost does not emit visible light, which is the so-called "stealth effect". The reason for this phenomenon is that the flame temperature of III-1 is very low, and in fact, the low flame temperature also results in the infrared radiation of III-1 being of very low intensity. Thus, the composite using only KNO₃ as the oxidizer has a good stealth effect, but its infrared radiation is not sufficient to meet the requirements of nighttime reconnaissance.



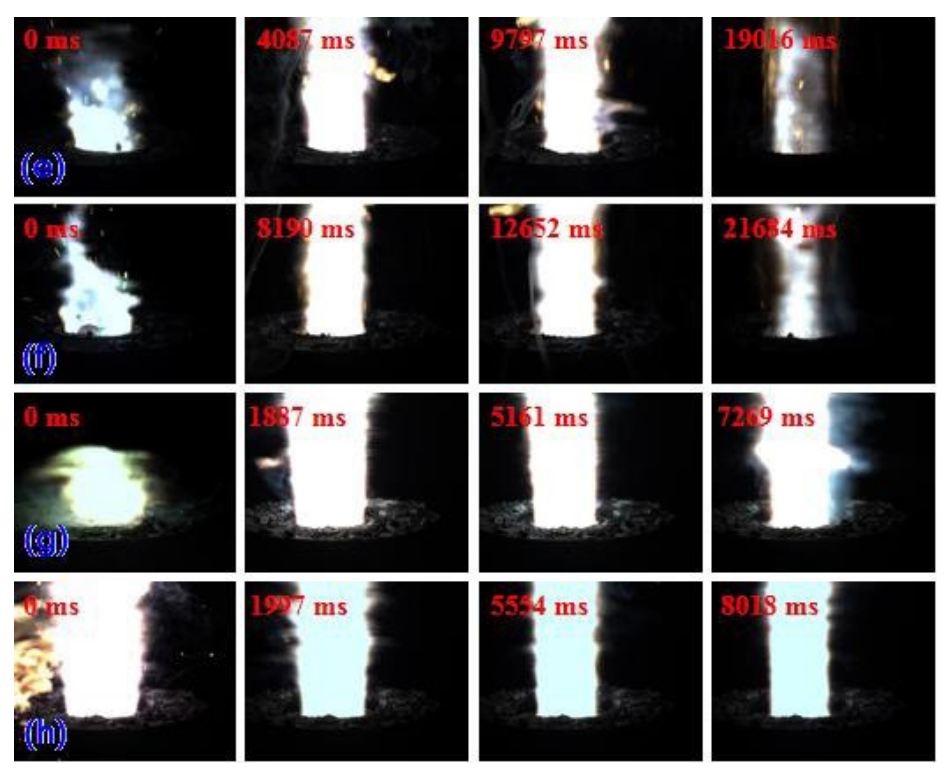


Figure 10. Flame photos and color spectra of red light composites: III-1(a), III-2 (b), III-3 (c), III-4 (d), III-5 (e), III-6 (f), III-7 (g) and III-8(h)

In the photos of the other seven composites, from the perspective of visible light, there are no significant differences in color or structure among the flames produced by their combustion, *i.e.* almost all the flames are white. Moreover, when the burning rate of a composite is high, its flame is thicker, and its color is whiter. Notably, we can infer from the spectra and chromatograms (Figure 7) that this white flame is not caused by the continuous spectrum generated by incandescent solid or liquid particles but by the emission of light from gaseous compounds in various wavelength ranges (380-720 nm). Therefore, as predicted in Table 2, although the flame temperature is not high, the complex gaseous combustion products lead to a white color in the flames. Therefore, further improving the stealth effect of combustion is difficult.

4 Conclusions

- On the basis of the current experimental results, infrared illuminants doped with K, Rb, and/or Cs ionic salt(s) have better infrared radiation effects and poor visible light emission effects.
- ♦ The experimental data show that the composite with only KNO₃ as the oxidizer burned for a long time with almost no visible light emission, but its infrared radiation was also much lower.
- ♦ When KClO₄ was used instead of KNO₃, the infrared radiation intensity suddenly increased, but the combustion duration was only half that of KNO₃.
- ♦ The addition of RbNO₃ expanded the range and intensity of infrared radiation; hence, RbNO₃ is an excellent oxidizer and infrared radiation source in infrared illuminants. In particular, the combination of RbNO₃ and KNO₃ can produce extremely strong infrared radiation.
- ♦ The addition of CsNO₃ further expanded the wavelength range of infrared radiation and did not have a negative effect on the intensity of the infrared radiation. However, the combustion rates of composites containing Cs₂CO₃ were significantly higher, and the flame temperatures were slightly lower. Therefore, the effect of Cs₂CO₃ is not as good as that of CsNO₃.
- ♦ Overall, when the composite simultaneously contained KNO₃, KClO₄, RbNO₃, and CsNO₃, the infrared radiation generated by its combustion was the strongest, and the wavelength range was the widest. Therefore, the comprehensive use of potassium, rubidium, and cesium salts is an effective way to improve infrared radiation and reduce the visible light emission of composites. The data herein have guiding significance for our future work.

References

- [1] Koch, E.-C.; Hahma, A.; Weiser, V.; Roth, E.; Knapp, S. Metal-Fluorocarbon Pyrolants. XIII: High Performance Infrared Decoy Flare Compositions based on MgB₂ and Mg₂Si and Polytetrafluoroethylene/Viton®. *Propellants Explos. Pyrotech.* **2012**, *37*(4): 432-438; https://doi.org/10.1002/prep.201200044.
- [2] Matula, T.J.; Guan, J.; Crum, L.A. Near-Infrared Emissions in Single-Bubble and Multibubble Sonoluminescence. *Phys. Rev. E* **2001**, *64* paper 026310; https://doi.org/10.1103/PhysRevE.64.026310.
- [3] Kim, H.S.; Wagner, D.R.; Saykally, R.J. Single Photon Infrared Emission Spectroscopy of the Gas Phase Pyrene Cation: Support for a Polycyclic Aromatic Hydrocarbon Origin of the Unidentified Infrared Emission Bands. *Phys. Rev. Lett.* **2001**, *86*(25): 5691-5694; https://doi.org/10.1103/PhysRevLett.86.5691.

- [4] Trung, T.N.; Thi Cam, N.N. Effects of Mg-Al Alloy Powder on the Combustion and Infrared Emission Characteristics of the Mg-Al/PTFE/Viton Composition. *Def. Sci. J.* **2020**, *70*(6): 590-595; https://doi.org/10.14429/dsj.70.15522.
- [5] Conkling, J.A.; Mocella, C.J. *Chemistry of Pyrotechnics: Basic Principles and Theory*, 3rd Ed., CRC Press, Taylor & Francis Group, **2019**; ISBN: 9780429262135.
- [6] Streyer, W.; Feng, K.; Zhong, Y.; Hoffman, A.J.; Wasserman, D. Selective Absorbers and Thermal Emitters for Far-Infrared Wavelengths. *Appl. Phys. Lett.* **2015**, *107*(8) paper 081105; https://doi.org/10.1063/1.4929432.
- [7] Debnath, S.; Rej, P.; Kumar, H.; Jain, S.; Banerjee, S. A Computational Model for Prediction of IR Intensity and Burn Time of Magnesium-Teflon-Viton (MTV) based Infrared (IR) Decoy Flare of Various Configurations. *Infrared Phys. Technol.* **2025**, *145* paper 105651; https://doi.org/10.1016/j.infrared.2024.105651.
- [8] Elbasuney, S.; Elsaidy, A.; Kassem, M.; Tantawy, H.; Sadek, R.; Fahd, A. Infrared Spectra of Customized Magnesium/Teflon/Viton Decoy Flares. *Combust. Explos. Shock Waves* 2019, 55(5): 599-605; https://doi.org/10.1134/S0010508219050113.
- [9] Elbasuney, S.; Elmotaz, A.A.; Sadek, M.A.; Tantawy, H.; Yehia, M.; El-Sayyad, G.S. Reduced Graphene Oxide: A Novel Black Body Emitter for Advanced Infrared Decoy Flares. *J. Energ. Mater.* 2021, 39(1): 100-112; https://doi.org/10.1080/073 70652.2020.1762800.
- [10] Bhoyar, R.A.; Choubey, S.R.; Wankhede, S.P.; Belsare, P.D.; Moharil, S.V. Near-Infrared Emission in Bi₃ScMo₂O₁₂. *Radiat. Eff. Defects Solids* **2024**, 179(5-6): 686-694; https://doi.org/10.1080/10420150.2024.2304191.
- [11] Yu, S.; Fu, L.; Zhou, Y.; Su, H. Novel Bifunctional Magnetic-Near-Infrared Luminescent Nanocomposites: Near-Infrared Emission from Nd and Yb. *Photochem. Photobiol. Sci.* **2011**, *10*(4): 548-553; https://doi.org/10.1039/C0PP00293C.
- [12] Kshetri, Y.K.; Joshi, B.; Diaz-Torres, L.A.; Lee, S.W. Efficient Near Infrared to Visible and Near-Infrared Upconversion Emissions in Transparent (Tm³+, Er³+)-α-Sialon Ceramics. *J. Am. Ceram. Soc.* 2017, 100(1): 224-234; https://doi.org/10.1111/jace.14573.
- [13] Guo, Z.; Rui, T.C.; Yu, C.; She, Y.D.; Liang, Z.; Xing, H.L.; Yuan, R.J.; Wei, H.G. Upconversion Luminescent NaYbF₄: Er³⁺, Tm³⁺ Nanoparticles: Spectrally Pure and Intense Near Infrared to Near Infrared Emission. *J. Nano Res.* **2015**, *33*: 83-91; https://doi.org/10.4028/www.scientific.net/JNanoR.33.83.
- [14] Lv, Y.; Li, Y.; Li, Z.; Xie, R. Near-Infrared Emission of Sm²⁺ in Oxynitrides. *Adv. Opt. Mater.* **2024**, *12*(10) paper 2302303; https://doi.org/10.1002/adom.202302303.
- [15] Lezhnina, M.; Laeri, F.; Benmouhadi, L.; Kynast, U. Efficient Near-Infrared Emission from Sodalite Derivatives. Adv. Mater. 2006, 18(3): 280-285; https://doi.org/10.1002/adma.200501206.
- [16] Sajid, S.; Animesh, G.; Radha, R.; Aprajita, J.; Priolkar, K.R.; Surajit, S.; Santra, P.K.; Kadhiravan, S.; Angshuman, N. Ultrabroad Near Infrared Emitting Perovskites. Angewandte Chemie-International Edition 2025, 64(2) paper e20241500; https://doi.org/10.1002/anie.202415003.

- [17] van Damme, I.M.; Mestres-Fitó, P.; Ramaker, H.J.; Hulsbergen, A.W.C.; van der Heijden, A.E.D.M.; Kranenburg, R.F.; van Asten, A.C. Rapid and On-Scene Chemical Identification of Intact Explosives with Portable Near-Infrared Spectroscopy and Multivariate Data Analysis. *Sensors* **2023**, *23*(8) paper 3804; https://doi.org/10.3390/s23083804.
- [18] Majewska, N.; Tsai, Y.T.; Zeng, X.Y.; Fang, M.H.; Mahlik, S. Advancing Near-Infrared Light Sources: Enhancing Chromium Emission through Cation Substitution in Ultra-Broadband Near-Infrared Phosphors. *Chem. Mater.* 2023, 35(23): 10228-10237; https://doi.org/10.1021/acs.chemmater.3c02466.
- [19] Fischer, N.; Feller, M.; Klapoetke, T.M.; Kowalewski, M.; Scheutzow, S.; Stierstofer, J. Spectroscopic Investigations of High-Nitrogen Compounds for Near-Infrared Illuminants. *Propellants Explos. Pyrotech.* 2014, 39(2): 166-172; https://doi.org/10.1002/prep.201300092.
- [20] Jeevaraj, M.; Sivaganesh, D.; Saravanakumar, S.; Asath Bahadur, S.; Sudhahar, S.; Krishna Kumar, M. Broadband Near Infrared Emission in Cr³⁺: Cs₂AgBiCl₆ Double Perovskite Halides. *Opt. Mater.* 2023, 143 paper 114294; https://doi.org/10.1016/j. optmat.2023.114294.
- [21] Bouma, R.H.B.; Kotter, L.N.; Smit, W.J.L.; Zebregs, M.; Groven, L.J. Mixed Colors by Combustion of Mixed Homogeneous Pyrotechnics and Heterogeneous Charges. *Propellants Explos. Pyrotech.* 2024, 49(3) paper e202300218; https://doi.org/10.1002/prep.202300218.
- [22] Yi, W.; Xiaolan, S.; Dan, S.; Li, L.; Chongwei, A.; Jingyu, W. Synthesis, Thermolysis, and Sensitivities of HMX/NC Energetic Nanocomposites. *J. Hazard. Mater.* **2016**, *312*: 73-83; https://doi.org/10.1016/j.jhazmat.2016.03.043.

Authorship contribution statement

Yi Wang: conception, foundations, methods, performing the

experimental part, performing the statistical analysis

Xiaolan Song: methods, performing the experimental part

Chongwei An: performing the statistical analysis, other contribution to the

publication

Fengsheng Li: conception, methods, other contribution to the publication

Submitted: December 19, 2024 Revised: September 29, 2025

First published online: September 30, 2025